High-pressure phase transitions of α-quartz under non-hydrostatic dynamic conditions: A reconnaissance study at PETRA III

Eva-Regine CARL[1,4*], Ulrich MANSFELD [2], Hanns-Peter LIERMANN [3], Andreas DANILEWSKY [4], Falko LANGENHORST [2], Lars EHM [5,6], Ghislain TRULLENQUE [7], André ROTHKIRCH [3], and Thomas KENKMANN [1]

[1] Institut für Geo- und Umweltnaturwissenschaften, Geologie, Albertstr. 23b, Albert-Ludwigs-Universität, 79104 Freiburg, Germany
[2] Institut für Geowissenschaften, Mineralogie, Carl-Zeiss-Promenade 10, Friedrich-Schiller-Universität Jena, 07745 Jena, Germany
[3] DESY, Notkestraße 85, 22607 Hamburg, Germany
[4] Institut für Geo- und Umweltnaturwissenschaften, Kristallographie, Hermann-Herder-Str. 5, Albert-Ludwigs-Universität, 79104 Freiburg, Germany
[5] Stony Brook University, Mineral Physics Institute, Stony Brook, NY 11794-2100, USA
[6] National Synchrotron Light Source II, Brookhaven National Laboratory, Upton, NY 11973-500, USA
[7] Institut Polytechnique LaSalle Beauvais, Departement GEOS, équipe B2R 19 rue Pierre Waguet - BP 30313 - 60026 BEAUVAIS Cedex, France

*Corresponding author. E-mail: eva-regine.carl@geologie.uni-freiburg.de

Abstract- Hypervelocity collisions of solid bodies occur frequently in the solar system and affect rocks by shock waves and dynamic loading. A range of shock metamorphic effects and high-pressure polymorphs in rock-forming minerals are known from meteorites and terrestrial impact craters. Here we investigate the formation of high-pressure polymorphs of α-quartz under dynamic and non-hydrostatic conditions and compare these disequilibrium states with those predicted by phase diagrams derived from static experiments under equilibrium conditions. We create highly dynamic conditions utilizing a membrane-driven diamond anvil cell and study the phase transformations in α-quartz *in-situ* by synchrotron powder x-ray diffraction. Phase transitions of α-quartz are studied at pressures up to 66.1 GPa and different loading rates. At compression rates between 0.14 and 1.96 GPa/s, experiments reveal that α-quartz is amorphized and partially converted to stishovite between 20.7 GPa and 28.0 GPa. Therefore, coesite is not formed as would be expected from equilibrium conditions. With increasing compression rate, a slight increase of the transition pressure occurs. The experiments show that dynamic compression causes an instantaneous formation of structures consisting only of SiO_6-octahedra rather than the rearrangement of the SiO_4-tetrahedra to form coesite. Although shock compression rates are orders of magnitude faster, a similar mechanism could operate in impact events.

INTRODUCTION

Quartz is an omnipresent mineral in near-surface rocks of the continental lithosphere and, therefore, among the best studied phases under equilibrium conditions. Its wide occurrence also makes it the most widely used shock barometer (Stöffler and Langenhorst 1994; French and Koeberl 2010) in impact studies.

High-pressure polymorphs of α-quartz such as coesite (Coes 1953) are known from different geologic settings. For example, natural occurrences of coesite were first reported from impact craters, namely Meteor crater, AZ, USA (Chao et al. 1960) and the Ries crater, Germany (Chao and Shoemaker 1961). Later on, coesite was found in mantle derived kimberlites (e.g., Smyth et al. 1977), and in ultra-high-pressure metamorphic rocks of continental collision zones (e.g., Chopin 1984).

The thermodynamic stability fields of high pressure polymorphs of α-quartz have been experimentally and theoretically investigated since 1953 (Coes 1953): α-Quartz transforms to coesite with four-fold coordinated Si at 2 GPa and to stishovite with six-fold coordinated Si (Stishov et al. 1961) at 8 GPa (Kirfel et al. 2001) and room temperature. At quasi-hydrostatic conditions and room temperature, the high-pressure polymorphs coesite I and coesite II have also been reported (Černok et al. 2014).

However, a great mismatch exists when the static stability field of high-pressure SiO_2-polymorphs is compared to the occurrence of these phases during shock metamorphism. In impact craters, coesite is found only in diaplectic SiO_2 glasses that were exposed to shock pressures in excess of 35 GPa, e.g., Stöffler and Langenhorst (1994). Coesite is thought to crystallize exclusively upon shock pressure release from silica melt (Stöffler and Langenhorst 1994; Langenhorst and Deutsch 2012; Fazio et al. 2016). Stishovite, on the other hand, is believed to form via a solid-solid transition during shock compression at lower pressures than coesite (French and Koeberl 2010) and then reverts back to the amorphous state (Luo et al. 2003). Considering the high-energy barrier of a solid-solid phase transition to stishovite, however, a nucleation of stishovite from hot spots of silica melt is also suggested as a further hypothesis for the formation of stishovite. The occurrence of stishovite in melt pockets (Kieffer et al. 1976; Mansfeld et al. 2016) or melt veins (Langenhorst and Poirier 2000) supports this hypothesis. Hence, the formation and preservation of coesite and stishovite depends on the specific pressure-temperature evolution during shock compression and decompression.

Furthermore, diamond anvil cell experiments reveal a complex behavior of α-quartz under compression (e.g., Dubrovinsky et al. 2004). Reconstructive phase transitions to the stable high-pressure polymorphs are often hindered by high kinetic barriers resulting in formation of complex metastable phases if heating is not sufficient (e.g., Choudhury et al. 2006). In the following, we briefly review literature data of SiO_2 high-pressure polymorphs, which is relevant for the interpretation of our results.

Under dynamic compression, α-quartz undergoes a pressure-induced amorphization in the pressure range 18 – 35 GPa (McNeil et al. 1992; Kingma et al. 1993a; Kingma et al. 1993b). Furthermore, theoretical investigations of the SiO_2 system predict a number of competing metastable post-quartz phases that precede or coexist along the full amorphization (Choudhury et al. 2006; Teter et al. 1998; Wentzcovitch et al. 1998) indicating that the structural transformation pathways are highly dependent on the precursor phase and the degree of hydrostaticity (Ohtaka et al. 2001; Huang et al. 2006; Haines et al. 2000).

Quartz ($P3_221$ space group) may transform to a monoclinic ($P2_1/c$ space group) post-quartz phase (Haines et al. 2001). Its structure is built of 3 x 2 kinked chains of edge-sharing SiO_6-octahedra. Theoretical calculations by Teter et al. (1998) and Martoňák et al. (2007) reveal that this phase transformation is diffusionless. The monoclinic post-quartz phase has not been discovered in natural geological settings. This phase is closely related to stishovite ($P4_2/mnm$ space group) that is built of edge-sharing octahedra forming straight chains. These two structures are competing because of very similar activation energies (Teter et al. 1998). Furthermore, there are many analogous structures that feature chains of edge-sharing octahedra with different kinking sequences such as seifertite (2 x 2 kinked chains) or SnO_2-type SiO_2 (4 x 4 kinked chains). Besides the transition from α-quartz to the monoclinic post-quartz phase, the formation of intermediate and metastable phase quartz II was reported (Choudhury et al. 2006). Quartz II forms above 16 GPa and co-exists with the monoclinic post-quartz phase (Haines et al. 2001; Prakapenka et al. 2004). The structure of quartz II is calculated to be monoclinic (C2 space group) and characterized by mixed polyhedral building blocks: Two-thirds of the silicon atoms are in octahedral coordination, while the remaining one-third is tetrahedrally coordinated. This C2 structure is built up of edge-shared octahedral units with corner-shared silicate tetrahedra, which form a framework structure. Computations by Choudhury et al. (2006) show that quartz II can form at 9 GPa with α-quartz persisting metastably up to 32 GPa.

Due to the great complexity (e.g., influence of the precursor phase) and to the metastability of high-pressure SiO_2 phases, previous investigations on α-quartz at high pressure have left many unanswered questions concerning the behavior of the material and the evolution of high-pressure phases.

Here we present time-resolved X-ray diffraction experiments under dynamic compression that provide insights into the kinetics of high-pressure phase transitions of α-quartz, making use of fast data acquisition now available at synchrotrons. Although the compression rates are much higher and temperatures are elevated in the context of impact cratering, these *in-situ* investigations of phase transitions are a necessary first step to understand the behavior of SiO_2 under the much faster compression rates of impact events. The obtained diffraction patterns are compared to transmission electron microscopic (TEM) observations of recovered samples.

EXPERIMENTAL METHODS

The experiments were conducted in a membrane-driven diamond anvil cell (mDAC), which was equipped with diamonds of a culet size of 0.3 mm. The culets indented 0.25 mm Re-gaskets to 0.020 – 0.035 mm thickness before a 0.1 mm hole was drilled at its center. A mixture of α-quartz powder (Alfa Aesar, 99.5%, -400 Mesh, 2 Micron, LOT: L01W019) and Au flakes as an internal pressure calibration (about 1 wt. %) was filled into to the gasket hole without a pressure medium.

Monochromatic X-ray powder diffraction experiments were carried out at the Extreme Conditions Beamline (ECB) P02.2 at PETRA III, DESY, Hamburg, Germany (Liermann et al. 2015). The wavelength was tuned to 0.28985 Å for the experiment SiO_2_RT_01 and to 0.29135 Å for the four experiments SiO_2_RT_03, 05, 06 and 09. The recorded diffraction patterns were too weak for an unambiguous identification of the high-pressure phases. In order to improve to quality of the diffraction patterns, the energy of the beam was switched from 42.7 keV to 25.6 keV. These experiments SiO_2_RT_02, 04, 07 and 08 were carried out at a wavelength of 0.48374 Å (Table 1). The sample to detector distance was calibrated using the CeO_2 standard (NIST 687) and varied between 369.13 mm (SiO_2_RT_01), 449.81 mm (SiO_2_RT_03, 05, 06 and 09), and 431.12 mm (SiO_2_RT_02, 04, 07 and 08). The X-ray beam was focused with either Kirkpatrick-Baez mirrors (2 x 2 μm^2 focus) or Compound Refractive Lens systems (8 x 3 μm^2 focus). The compression and decompression was achieved by pumping He-gas into or out of

the membrane after activation of the membrane pressure controller. Identical rates for compression and decompression rates were defined but friction between the piston and cylinder of the mDAC caused slower rates on the sample during decompression. During compression and decompression, diffraction images were taken every one (fast compression) to ten (slow compression) seconds. They were recorded on a Perkin Elmer area detector (model XRD 1621) and were subsequently converted to one-dimensional diffraction diagrams using the software Fit2D (Hammersley et al. 1996).

The experimental data were surveyed using the P02 Processing Tool (Konopkova et al. 2015; Rothkirch 2014, personal communication). This software provided an online tool to quickly process and plot the one-dimensional diffraction patterns as a function of frame number and, thus, time to create two- and three-dimensional contour plots. The tool was essential to get an overview of the compression experiment to define the onset of phase transitions. For a detailed analysis of the diffraction patterns including the identification of phases and the determination of cell parameters, we used the program package FullProf (Rodríguez-Carvajal 1993).

The LeBail analysis (LeBail et al. 1988) was carried out from 3 to 15° 2θ for all diffraction patterns. The LeBail method extracts integrated intensities from powder diffraction data. Therefore, the structural factor and associated structural parameters are not needed to be known for a LeBail analysis. The algorithm involves the refinement of the unit cell, profile parameters, and intensities of the reflections to match the experimental diffraction pattern. For each phase, the lattice parameters and the width of the reflections at half maximum (FWHM) were refined using the split pseudo-Voigt function. Given that each experiment consists of between 1,500 and 3,690 diffraction patterns, a sequential fitting was carried out if possible.

The 100 and 101 reflection of α-quartz were fitted independently using the Rietveld method (Rietveld 1967, 1969) in order to obtain the integrated intensities of the reflections. These integrated intensities were used to determine the start and progress of the amorphization of the sample during compression. A decrease of the integrated intensity defines the start of the amorphization. An increase in the background or the typical “glass” hump at low diffraction angles cannot be observed in high-pressure experiments due to the dominant background arising from the DAC.

The transition pressures of the phase transitions are determined with respect to the appearance of the strongest reflection of the phase for all experiments. For stishovite, this is the 110 reflection.

After inspection of the X-ray diffraction pattern, three phases were further considered: α-quartz, monoclinic post-quartz phase, and stishovite. The starting lattice parameters were a = 4.91239 ± 4e-05 Å and c = 5.40385 ± 7e-05 Å for α-quartz (Will et al. 1988), a = 4.1773 Å and c = 2.6655 Å for stishovite (Hill et al. 1983) and a = 7.66 Å, b = 4.10Å, c = 5.03 Å and β = 117.9° for the monoclinic post-quartz phase (Haines et al. 2001). The unit cell dimensions computed from the 111, 200, 220 and 311 diffraction lines of gold were used to calculate the pressure using a third order Birch-Murnaghan Equation of State (Birch 1951) with the bulk modulus from Anderson et al. (1989).

The parameters of the compression cycle of nine experiments are listed in Table 1. The compression rates increased from 0.14 GPa/s to 1.96 GPa/s with increasing numbering of the experiments. In some experiments, the compression started at elevated pressure P_{start} due to too strong closing of the mDAC. The maximum pressure P_{max} ranged between 26.7 GPa (SiO_2_RT_04) and 66.1 GPa (SiO_2_RT_05) and was held constant for up to two hours (Table 1). Decompression did not reach ambient pressures but stopped at P_{end} due to the friction between the piston and the cylinder of the mDAC. The error in pressure is 0.5 GPa.

Table 1. The experimental conditions of the nine selected experiments SiO_2_RT_01 - SiO_2_RT_09.

SiO_2_RT_x	P_{start} [GPa]	Compression rate [GPa/s]	P_{max} [GPa]	Hold at P_{max} [min]	**Decompression rate [GPa/s]**	P_{end} [GPa]	Wavelength [Å]
01	0.0001	0.14	59.2	60	0.08	16.4	0.28985
02	0.0001	0.20	26.7	120	0.005	11.5	0.48374
03	6.4	0.34	57.1	10	0.13	43.0	0.29135
04	0.0001	0.55	37.5	120	0.15	26.4	0.48374
05	1.2	0.79	46.4	10	0.10	36.7	0.29135
06	3.0	1.02	51.0	10	0.10	44.1	0.29135
07	0.0001	1.02	50.4	120	[a]	[a]	0.48374
08	0.0001	1.69	36.6	120	0.15	8.5	0.48374
09	7.1	1.96	66.1	10	0.15	41.8	0.29135

[a] Diamonds broke during compression.

The identification of phases in the experiments was difficult because the non-hydrostatic compression caused high stresses on the grains that result in broadening of the reflections. Moreover, the weak scattering of α-quartz and the strong Compton scattering of the diamonds decreased the signal-to-noise ratio. Consequently, a LeBail-analysis reached its limit and the position of the low intensity reflections could not be determined precisely. They differed

strongly from one refinement step to the next or remain at positions where no reflection was observed.

For TEM investigations, the recovered sample of SiO_2_RT_4 was pushed out of the gasket with a needle. Fragments were then ground between two glass substrates and subsequently dispersed on a lacey carbon grid. TEM imaging and electron diffraction were carried out using a 200 kV FEI Tecnai G^2 (University Jena).

RESULTS

Figure 1a depicts a representative data set of a slow-compression experiment (SiO_2_RT_01) as a contour plot of integrated diffraction patterns. The corresponding pressure time curve is shown on Figure 1b.

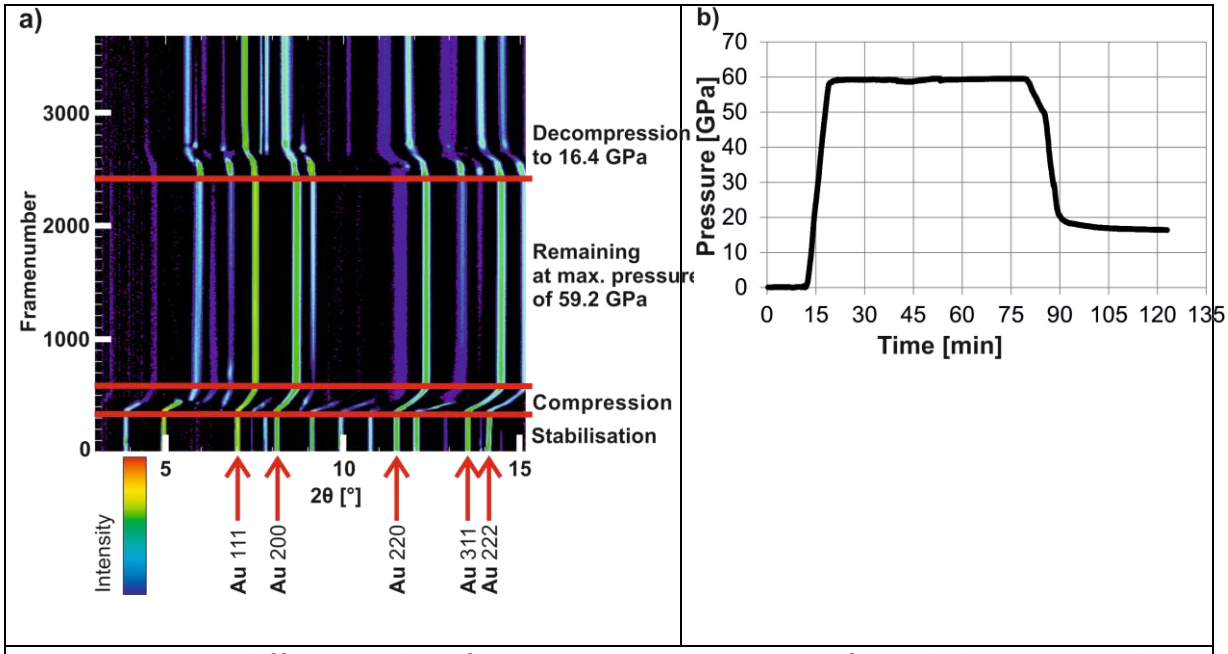

Figure 1. (a) 3D diffraction plot of experiment SiO_2_RT_01: After stabilization at ambient conditions, the compression of the material starts with a rate of 0.14 GPa/s. Then the maximum pressure of 59.2 GPa is maintained for 60 minutes. The final decompression of the material reaches 16.4 GPa. The pressure is obtained with respect to gold (Au). (b) The pressure-time-path of experiment SiO_2_RT_01 is shown.

No diffraction signal of coesite was observed in any of the compression experiments. The main feature observed in all experiments is the significant drop of the integrated intensity of the reflections of α-quartz between 10 and 15 GPa until complete disappearance. This is attributed to the amorphization of α-quartz. During amorphization, we also observe broadening of the reflections due to a reduction of the crystallite size and/or an increase in lattice distortion of α-quartz. Above 20 GPa, α-quartz transforms to the high-pressure phase stishovite as evident by the appearance of the 110, 211, 220, 310 and 002 reflections (Fig. 2).

Besides these major phase changes, we observe the appearance of additional diffraction lines that cannot be explained by contamination (e.g., Re-gaskets) and seem to be a feature of the compressed sample. In all runs, we see at low 2θ-values from 3° to 8° two reflections that can

be indexed with the strongest 111 and $\bar{2}11$ reflections of the monoclinic post-quartz (Fig. 2). These reflections appear at low pressures. Between 19 - 20 GPa, another weak reflection becomes visible in runs SiO_2_RT_01, _07, and _08 at 2θ values of 4 to 5 °2θ (Fig. 2). It is noteworthy that the appearance of the 111 and $\bar{2}11$ reflections goes along with an intensity drop in the Au 111 diffraction line indicating the compaction of the sample at the onset of the compression cycle. The 111 and $\bar{2}11$ reflections of the monoclinic post-quartz phase are present in all runs at highest pressure of the compression cycle.

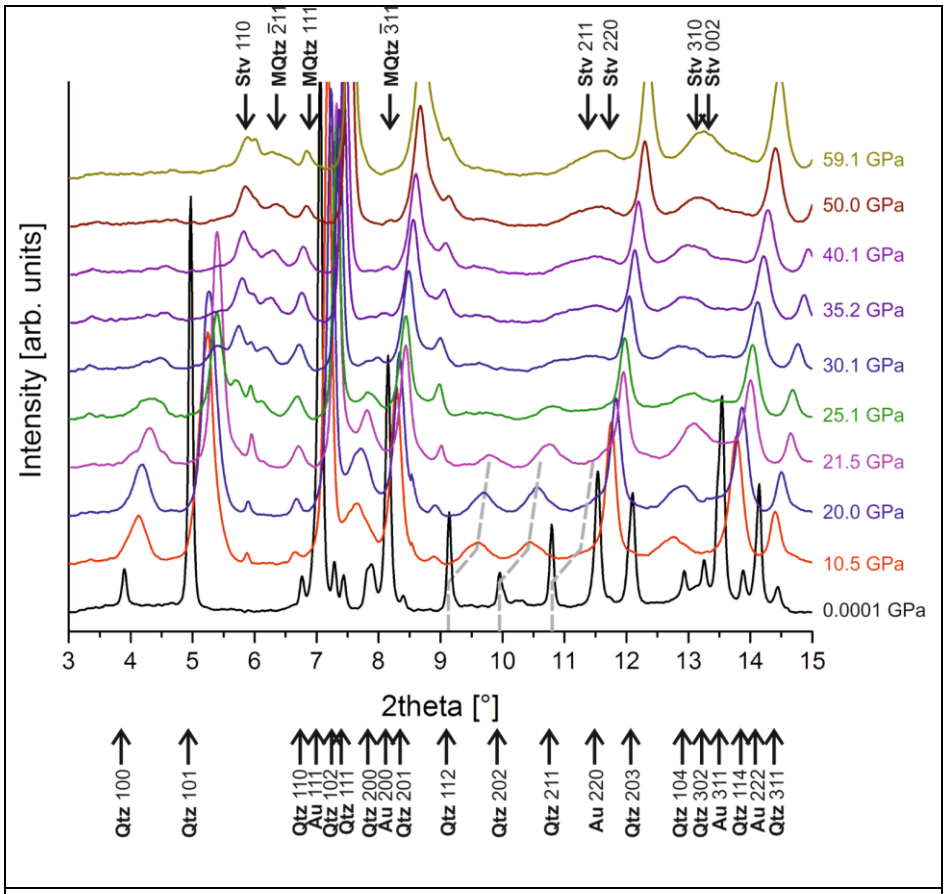

Figure 2. The evolution of the silica phases during compression in experiment SiO_2_RT_01 (compression rate: 0.14 GPa/s): The amorphization of α-quartz (Qtz) starts at around 10 GPa. Reflections of stishovite (Stv) occur at 20.7 GPa. At low pressures, two reflections are observed which could be interpreted as the $\bar{2}11$ and 111 reflections of the monoclinic post-quartz phase (MQtz). The pressure is obtained with respect to gold (Au).

There are no clear indications about a dependency of the pressure of stishovite formation on the compression rates with errors of ± 2 GPa for the pressure being relatively large. The transition

pressure ranges between 20.7 and 28.0 GPa considering compression rates up to 1.96 GPa/s. However, we observed significant lower transition pressures in the experiments SiO_2_RT_01, _07 and 08 that show the appearance of an additional weak reflection between 4 and 5° 2θ. This might be an indication for different deformation paths during the compression cycle, possibly related to different strain fields in the sample.

Fig. 3a features a diffraction pattern collected at the highest pressure of 59.2 GPa. Gold, stishovite, and the monoclinic post-quartz phase can be identified. The broad nature of the diffraction lines and their low intensity in comparison to the background indicate the large degree of amorphisation and the limited long-range order of the sample. After remaining at maximum pressure for 60 minutes, there are no significant changes observed in the diffraction pattern (Fig. 3b).

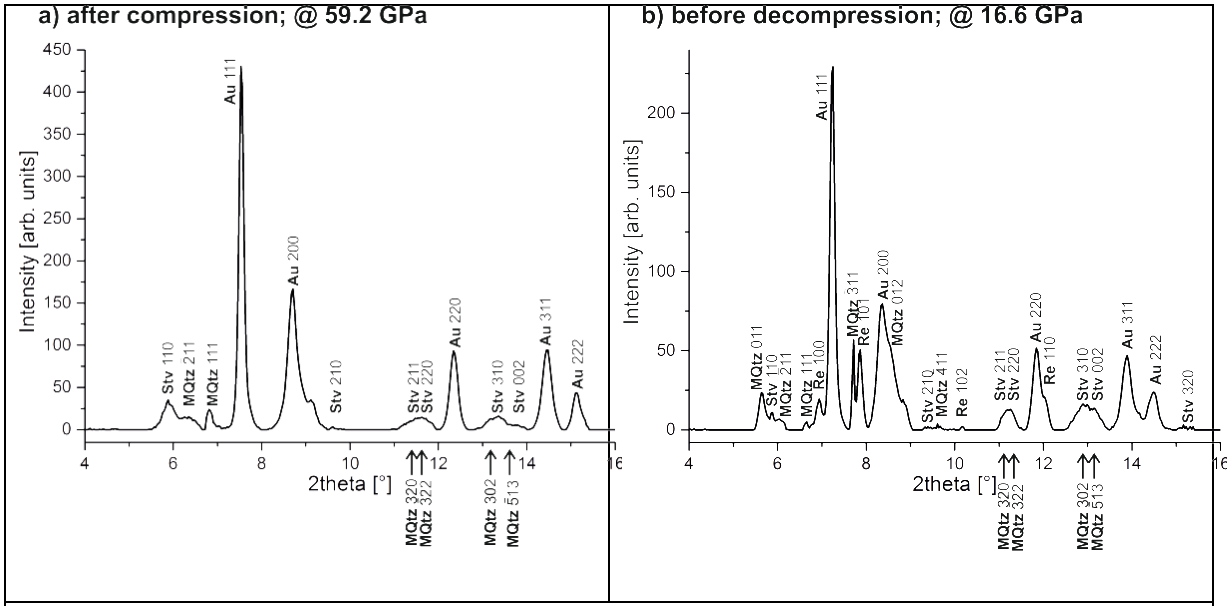

Figure 3. The evolution of the silica phases while remaining at the maximum pressure of 59.2 GPa. The pressure is obtained with respect to gold (Au). (a) After reaching maximum pressure, reflections of two silica phases are observed: stishovite (Stv) and the monoclinic post-quartz phase (MQtz). (b) After 60 minutes at maximum pressure, no changes are observed in the diffraction pattern. Collection time per diffraction pattern: 2 seconds.

During decompression, no further phase transition is observed (Fig. 4a). The reflections of stishovite and of the monoclinic post-quartz are observed down to the lowest minimum pressure of 16.5 GPa. Decompression did not reach ambient pressures because of the friction between

the piston and the cylinder of the mDAC. Due to a rearrangement of the powder and the movement of the gasket, additional reflections of the two silica phases and rhenium that originate from the gasket are observed (Fig. 4b).

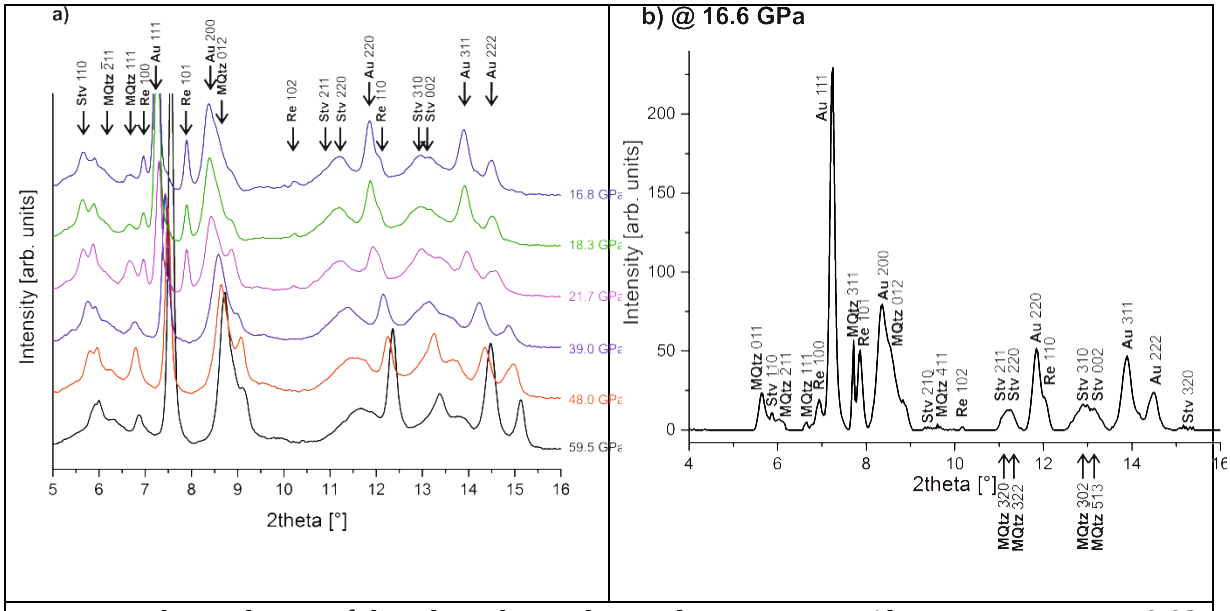

Figure 4. The evolution of the silica phases during decompression (decompression rate: 0.03 GPa/s). The pressure is obtained with respect to gold (Au). Due to a shift of the sample, reflections of rhenium (Re) from the gasket are also observed. (a) Stishovite (Stv) and the monoclinic post-quartz phase (MQtz) remain stable, while α-quartz does not reappear. At 49.9 GPa, the 011 reflection of the monoclinic post-quartz phase occurs. With the end of decompression, new reflections of the monoclinic post-quartz phase are observed. (b) A single diffraction pattern (collection time: 2 seconds) reveals the present phases at minimum pressure at 16.6 GPa. Stishovite and the monoclinic post-quartz phase are indicated. The overall intensity of the reflections of the silica phases has dropped.

The recovered sample of SiO_2_RT_04 was investigated by means of transmission electron microscopy (TEM). The microstructural investigation of a large number of fragments from the crushed specimen reveals that the vast majority of material was transformed to amorphous silica. Nonetheless, few regions contain small crystallites of stishovite embedded in the predominant amorphous silica as can be seen in Fig. 5. Using selected area electron diffraction (SAED), stishovite could be unambiguously identified on the basis of different zone axis patterns as shown in the insets in Fig 5. In the center image, linear alignments of crystallites

indicate a solid-state transition into stishovite. This is supported by the texturing of reflections in all electron diffraction patterns that were taken from numerous crystallites in a certain area indicating a preferred orientation of the crystallites. No other high-pressure phase of silica could be found by the TEM investigation of20-30 fragments of five samples each. However, the predominant observation of amorphous silica suggests that most of α-quartz is transformed to glass during the pressure evolution, while only a small amount of stishovite is formed which is in accordance with the low-intensity reflections of stishovite compared to the starting reflections of α-quartz in the synchrotron experiments. The monoclinic post-quartz phase could not be found.

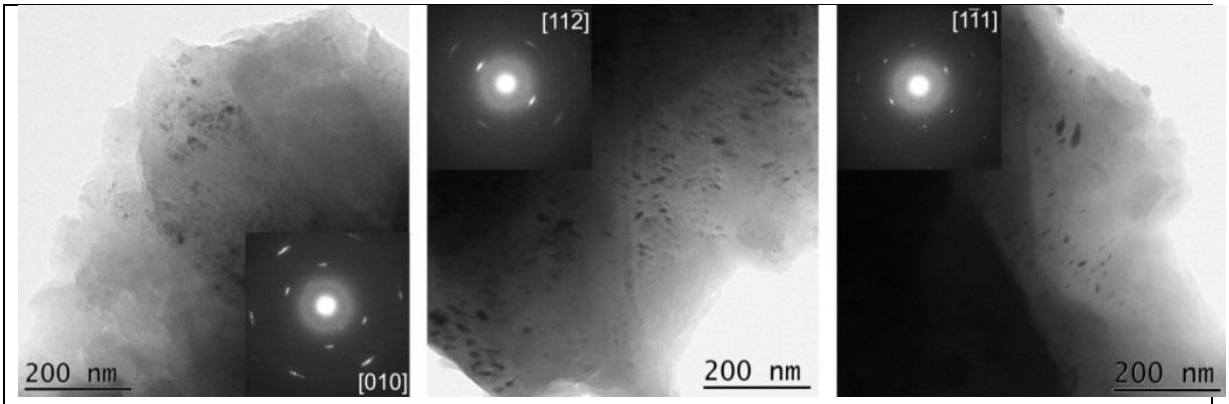

Figure 5. TEM images of the recovered sample of SiO_2_RT_04 show regions that contain crystallites of stishovite embedded in the predominant amorphous silica. The insets show diffraction patterns with characteristic zone axes of stishovite. The linear alignment of crystallites represented in the center image points to a solid-state transition into stishovite. This is supported by the texturing of reflections in the diffraction patterns taken over numerous crystallites indicating a preferred orientation of the crystallites.

DISCUSSION

The presented compression experiments on α-quartz clearly indicate a complex phase transition history. At low pressures, small parts of the sample seem to transform immediately to the monoclinic post-quartz phase, while it seems that the bulk of the sample does not transform until above 20 GPa. During the compression between 10-15 GPa, the bulk of the sample seems to amorphize as indicated by the broadening and drop of the intensities of the α-quartz diffraction lines as well as the increase in the background signal. This is further supported by

the analysis of the recovered samples with the TEM. The analysis reveals small crystallites of stishovite in an amorphous matrix, underlining that the mixture of amorphous portions and the monoclinic post-quartz phase transforms directly to stishovite at higher pressures above 22 GPa, bypassing the stability field of coesite., The transition from α-quartz to the monoclinic post-quartz phase in the pressure range from 21-35 GPa has been observed in very slow (static) compression experiments at room temperatures by Kingma et al. (1993b) and Haines et al. (2001) and, thus, matches well with our observations of the transition of the bulk sample. The transformation of smaller portions of the sample at much lower pressure is somewhat puzzling. However, taking into account the fact that the appearance of the 111 and $\bar{2}11$ diffraction lines go along with a significant drop in diffraction intensity of gold could indicate that at the beginning the sample in the chamber is not well compressed and moves during the initial compaction. During this process, it could very well be that few larger grains are birding between the diamonds and experiencing much higher pressures than indicated by the pressure standard of gold and, consequently, transforming much earlier to the monoclinic post-quartz phase than the bulk of the sample. The monoclinic post-quartz phase could not be found by subsequent TEM analysis. Nevertheless, it is conceivable that the phase is metastable and, thus, did not survive the preparation of the recovered samples as their reflections were observed under ambient conditions after the experiments. The transition from the amorphous phase or portion of the monoclinic post-quartz phase to stishovite has never been observed at ambient conditions. Stishovite formation has only been observed at elevated temperatures, e.g., at 1000 K and 55 GPa by Prakepenka et al. (2004). However, simulations by Martoňák et al. (2007) showed that a direct transition from α-quartz to stishovite may be possible via the metastable phase quartz II that is thought to be the first phase whose structure contains SiO_6-octahedra forming between 16 GPa and 20 GPa (e.g., Prakapenka et al. 2004; Haines et al. 2001). Thus, it is conceivable that the monoclinic post-quartz phase can be seen as another intermediate state aiding the formation of SiO_6-octahedra and helping to induce the transition to stishovite.

In all experiments, up to three additional reflections were observed that could not be attributed to stishovite, the monoclinic post-quartz phase or possible contaminations. A distinct indexing of these reflections was not possible because the reflections could be attributed to more than one additional high-pressure phase of α-quartz such as seifertite or SnO_2-type SiO_2. Moreover, the low signal/noise ratio and the circumstance that the reflections of gold might overlap with important reflections make the identification of the phases even more difficult. However, taking the different kinking of SiO_6-octahedra between the high-pressure phases into account, the occurrence of these reflections may resemble a disordering in the monoclinic post-quartz phase.

On the other hand, the weak reflection between 4 and 5° 2θ might be the 001 reflection of quartz II, although no other observed reflections can be indexed for this phase. In general, these observations show the complexity of the non-hydrostatic compression in the mDAC.

The pressure-induced amorphization of α-quartz starts between 10 GPa and 15 GPa, which is below the range of 18 GPa to 35 GPa as obtained in earlier studies (McNeil et al. 1992; Kingma et al. 1993a; Kingma et al. 1993b). We suggest that increased strains in a non-hydrostatic compressed sample result in amorphization at lower pressures, especially when considering that McNeil et al. (1992) and Kingma et al. (1993a) used pressure-transmitting media for their experiments.

To conclude, we conducted nine compression experiments at varies compression rates indicating a transition of α-quartz to stishovite via an intermediate monoclinic post-quartz phase. The transformation to stishovite shows no rate dependency within the range explored in our experiments. This observation is in agreement with the observations from shock compression experiments on α-quartz (e.g., Fiske et al. 1998; Luo and Ahrens 2003).Recent in-situ laser shock experiments on silica glass showed the formation of stishovite as well, and are thus in line with this interpretation (Gleason et al. 2015). During decompression, stishovite and the monoclinic post-quartz phase stay stable to minimum pressure of the compression experiment, while no reflections of α-quartz are observed. In literature, α-quartz was reported to recrystallize (e.g., Haines et al. 2001; Kingma et al. 1993b). Haines et al. (2001) reported the monoclinic post-quartz phase and a small amount of α-quartz under ambient conditions. His assumption that quartz II recrystallizes to α-quartz during decompression helps excluding the formation of quartz II in our experiments because reflections of α-quartz were not observed under ambient conditions after the experiment.

SUMMARY

We use a combination of a membrane-driven diamond anvil cell and *in-situ* powder x-ray diffraction to study the phase transitions of α-quartz at pressures up to 66.1 GPa at room temperature and different compression rates up to 2.0 GPa/s. The collection time of one diffraction pattern is down to one second.

The non-hydrostatic compression experiments reveal that α-quartz transforms even at room temperature directly to stishovite, skipping the stability field of coesite. This observation

suggests that stishovite could possibly directly form during shock compression, which is much shorter but takes place at enhanced temperature. This phase transition to stishovite occurs in our experiments between 20.7 GPa and 28.0 GPa during compression and slightly increases with increasing compression rate. Stishovite remains stable upon reaching maximum pressure and during the time while the maximum pressure is kept for more than one hour. During decompression, stishovite reflections remain observable, while no reflections of α-quartz appear in the patterns. The formation of stishovite was confirmed by an analysis of the recovered samples in the TEM.

In the course of compression, new reflections can be observed up to 19.8 GPa, which might be assigned to the monoclinic post-quartz phase, although an independent proof of this phase by TEM analysis was not successful. These new reflections remain detectable until the maximum pressure is reached. The reflections are not influenced by the phase transition of α-quartz to stishovite. Upon decompression, these reflections do not vanish.

Furthermore, an amorphization of α-quartz starts between 10 GPa and 15 GPa during compression. The material becomes more and more amorphous with proceeding compression until α-quartz transforms to stishovite. The amount of stishovite formed is very small and its long range order decreases as shown by the weak and broad reflections of this phase. After the phase transition, the amorphization only progresses slightly forward as revealed by diffraction patterns taken at maximum pressures between 26.7 GPa and 66.1 GPa. There are no other changes with respect to the phases of silica observed in these diffraction patterns.

Our dynamic compression experiments provide insight into the kinetics of high-pressure phase transitions of α-quartz: The experiments indicate that an impact causes an instantaneous formation of structures consisting only of SiO_6-octahedra rather than the rearrangement of the SiO_4-tetrahedra to form coesite. Although the compression rates are much higher and temperatures are elevated in the context of impact cratering, these *in situ* investigations of phase transitions are a necessary first step to understand the behavior of SiO_2 under the much faster compression rates of impact events. The latter is envisaged to be studied with a laser shock compressed sample at x-ray free electron lasers (XFELs) in the future (Gleason et al. 2015).

ACKNOWLEDGEMENT

This study was conducted in the framework of the DFG research unit FOR-887 “Experimental Impact Cratering – The MEMIN II Program (Multidisciplinary Experimental and Modeling Impact Research Network), project KE 732/23-1 “Dynamic loading and unloading of SiO_2 aggregates. Real-time phase transformation monitored by means of synchrotron beam diffraction”. One of us (FL) is grateful to the Deutsche Forschungsgemeinschaft for funds provided by the Leibniz program (LA 830/14-1) and project LA830/17-1 within the MEMIN II program.

REFERENCES

Anderson O.L., Isaak D.G., and Yamamoto S. 1989. Anharmonicity and the equation of state for gold. *Journal of Applied Physics* 65: 1534-1543.

Birch F. 1952. Elasticity and constitution of the Earth’s interior. *Journal of Geophysical Research* 57: 227-286.

Černok A., Bykova E. Ballaran T.B., Liermann H.P., Hanfland M., and Dubrovinsky L. 2014. High-pressure crystal chemistry of coesite-I and its transition to coesite-II. *Zeitschrift für Kristallographie* 229: 761-773.

Choudhury N. and Chaplot S.L. 2006. Ad initio studies of phonon softening and high-pressure phase transitions of α-quartz SiO_2. *Physical Review B* 73: 094304.

Coes L. 1953. A new dense crystalline silica. *Science* 118: 131-132.

Dubrovinsky L.S., Dubrovinskaia N.A., Prakapenka V., Seifert F., Langenhorst F., Dmitriev V., Weber H.P., and Le Bihan T. 2004. A class of new high-pressure silica polymorphs. *Physics of the Earth and Planetary Interiors* 143-144: 231-240

Fazio A., Mansfeld U., and Langenhorst F. 2016. Coesite in suevite from the Ries impact structure (Germany): from formation to post-shock evolution. *Meteoritics & Planetary Science* this volume.

Fiske P.S., Nellis W.J., Xu Z., and Stebbins J.F. 1998. Shocked quartz: A ^{29}Si magic-angle-spinning nuclear magnetic resonance study. *American Mineralogist* 83: 1285-1292.

French B.M. and Koeberl C. 2010. The convincing identification of terrestrial meteorite impact structures: What works, what doesn’t, and why. *Earth-Science Reviews* 98: 123-170.

Gleason A.E., Bolme C.A., Lee H.J., Nagler B., Galtier E., Milathianaki D., Hawreliak J., Kraus R.G., Eggert J.H., Fratanduono D.E., Collins G.W., Sandberg R., Yang W. and Mao W.L. 2015. Ultrafast visualization of crystallization and grain growth in shock-compressed SiO_2. *Nature Communications* 6: 8191.

Haines J., Léger J.M., and Chateau C. 2000. Transition to a crystalline high-pressure phase in α-GeO2 at room temperature. *Physical Review B* 61: 8701-8706.

Haines J., Léger J.M., Gorelli F., and Hanfland M. 2001. Crystalline post-quartz phase in silica at high pressure. *Physical Review Letters* 87: 155503.

Hammersley A.P., Svensson S.O., Hanfland M., Fitch A.N., and Häusermann D. 1996. Two-dimensional detector software: From real detector to idealized image or two-theta scan. *High Pressure Research* 14: 235-248.

Hill R.J., Newton M.D., and Gibbs G.V. 1983. A crystal chemical study of stishovite. Locality: synthetic. *Journal of Solid State Chemistry* 47: 185-200.

Huang L., Durandurdu M., and Kieffer J. 2006. Transformation pathways of silica under high pressure. *Nature Materials* 5: 977-981.

Kieffer S. W., Phakey P. P., and Christie J. M. 1976. Shock processes in porous quartzite; transmission electron microscope observations and theory, *Contributions to Mineralogy and Petrology* 59: 41–93.

Kingma K.J., Meade C., Hemley R.J., Mao H., and Veblen D.R. 1993(a). Microstuctural observations of α-quartz amorphization. *Science* 259: 666-669.

Kingma K.J., Hemley R.J., Mao H., and Veblen D.R. 1993(b). New high-pressure transformation in α-quartz. *Physical Review Letters* 70: 3927-3930.

Kirfel A., Krane H.G., Blaha P., Schwarz K., and Lippmann T. 2001. Electron-density distribution in stishovite, SiO_2: a new high-energy synchrotron-radiation study. *Acta Crystallographica section A* 57: 663-677.

Langenhorst F., and Poirier J.P. 2000. Anatomy of black veins in Zagami: Clues to the formation of high-pressure phases. *Earth and Planetary Science Letters* 184: 37-55

Langenhorst F., Deutsch A. (2012): Shock metamorphism of minerals. *Elements* 8(1), 31-36.

LeBail A., Duroy H., and Fourquet J.L. 1988. Ab initio structure determination of LiSbWO6 by x-ray powder diffraction. *Material Research Bulletin* 23: 447-452.

Liermann H.-P., Konôpková Z., Morgenroth W., Glazyrin K., Bednarcik J., McBride E.E., Petitgirard S., Delitz J.T., Wendt M., Bican Y., Ehnes A., Schwark I., Rothkirch A., Tischer M., Heuer J., Schulte-Schrepping H., Kracht T., and Franz H. 2015. The Extreme Conditions Beamline P02.2 and the Extreme Conditions Science Infrastructure at PETRA III. *Journal for Synchrotron Radiation* 22: 908 – 924.

Luo S., Ahrens T.J., and Asimov P.D. 2003. Polymorphism, superheating, and amorphization of silica upon shock wave loading and release. *Journal of Geophysical Research* 108: 2421.

Mansfeld U., Langenhorst F., Ebert M., Kowitz A., and Schmitt R.T 2016. Microscopic evidence of stishovite generated in low-pressure shock experiments on porous sandstone: constrains on its genesis. *Meteoritics and Planetary Science* this volume.

Martoňák R., Donadio D., Oganov A.R., and Parrinello M. 2007. From four- to six-coordinated silica: Transformation pathways from metadynamics. *Physical Review B* 014120: 1-11.

McNeil, L.E. and Grimsditch M. 1992. Pressure-amorphized SiO_2 α-quartz: An anisotropic amorphous solid. *Physical Reviews Letters* 68: 83-85.

Melosh H.J. 1989. *Impact Cratering*. New York: Oxford University Press. 245p.

Ohtaka O., Yoshiasa A., Fukui H., Murai K., Okube M., Katayama Y., Utsumi W., and Nishihata Y. 2001. Structural changes of quartz-type GeO2 under pressure. *Journal for Synchrotron Radiation* 8: 791-793.

Prakapenka V.P., Shen G., Dubrovinsky L.S., Rivers M.L., and Sutton S.R. 2004. High pressure induced phase transformation of SiO_2 and GeO_2: difference and similarity. *Journal of Physics and Chemistry of Solids* 65: 1537-1545.

Qiu Y.Z., Witek A., Onn D.G., Anthony T.R., and Banholzer W.F. 1993. Thermal conductivity of natural and synthetic diamonds with differing isotope contents. *Thermochimica Acta* 218: 257-268.

Rietveld, H.M. 1967. Line profiles of neutron powder-diffraction peaks for structure refinement. *Acta Crystallograohica* 22: 151 – 152.

Rietveld, H.M. 1969. A profile refinement method for nuclear and magnetic structures. *Journal of Applied Crystallography* 2: 65 – 71.

Rodríguez-Carvajal J. 1993. Recent advances in magnetic structure determination by neutron powder diffraction. *Physica B* 192: 55-69.

Sinclair W. and Ringwood A.E. 1978. Single crystal analysis of the structure of stishovite. *Nature* 272: 714-715.

Stishov S.M. and Popova S.V. 1961. A new dense modification in silica. *Geokhimiya* 10: 837-380.

Stöffler D. and Langenhorst F. 1994. Shock metamorphism of quartz in nature and experiment: I. Basic observation and theory. *Meteoritics and Planetary Science* 29: 155-181.

Teter D.M., Hemley R.J., Kresse G., and Hafner J. 1998. High-pressure polymorphs in silica. *Physical Review Letters 80*: 2145-2148.

Wentzcovitch R.M., da Silva C., Chelikowsky J.R., and Binggeli N. 1998. A new phase and pressure induced amorphization in silica. *Physical Review Letters* 80: 2149-2152.

Will G., Parrish W., and Hart M. 1988. Crystal structures of quartz and magnesium germinate by profile analysis of synchrotron-radiation high-resolution powder data. *Journal of Applied Crystallography* 21: 182-191.

Wünnemann K. and Ivanov B.A. 2003. Numerical modelling of impact crater depth-diameter dependence in an acoustically fluidized target. *Planetary and Space Science* 51:831-845.